

Determination of bubble diameters during pool boiling on surfaces with minichannels partially filled with porous elements

Norbert Dadas^{1,2*}, Robert Pastuszko^{1,2}, and Petra Dancova³

¹Kielce University of Technology, al. Tysiaclecia Panstwa Polskiego 7, PL-25-314 Kielce, Poland

²Central Office of Measures, ul. Elektoralna 2, 00-139 Warsaw, Poland

³Teplárna Liberec, a.s.. Dr. Milady Horákové 641/34a 460 01 Liberec, Czech Republic

Abstract. This article presents experimental studies conducted on enhanced surfaces in the form of minichannels partially filled with porous structures. The experiments were carried out during pool boiling of water for five different surfaces. For the tested samples as well as for the reference surfaces: minichannels without additional porous fillings (MC) and a plain surface, the heat flux and heat transfer coefficient were determined. All samples with additional fillings achieved higher heat fluxes and heat transfer coefficients with lower superheating compared to the MC and flat surface samples. Visualization of the boiling process was performed, enabling the measurement of the bubble diameters at the moment of detachment. Based on modified correlations from the literature, the diameters of the departure bubbles were determined and compared with the experimental data.

1 Introduction

The aim of this study was to conduct experimental research on heat transfer during pool boiling on minichannel surfaces with additional fillings in the form of wire meshes and metal foams. The diameters of the departing vapor bubbles were determined and compared with those calculated on the balance of forces acting on a detaching bubble. Such surfaces can be used as evaporators in cooling systems for components (e.g., processors) that generate large amounts of heat.

Pool boiling is one of the most complex processes among all heat transfer mechanisms [1]. Vapor bubbles are formed when the superheated liquid layer in contact with the heated surface reaches a sufficient thickness for the vapor pressure to overcome the surface tension forces and initiate bubble growth [2]. As the bubble grows, the buoyancy force increases, allowing the bubble to overcome surface tension. Once the resistance to surface tension is exceeded, bubble detachment from the heating surface begins. A more detailed analysis must also consider inertial forces, drag forces, and the force associated with pressure differences. The cyclic repetition of the bubble departure generates local liquid flows that induce convective motion within the liquid control volume. From a mechanistic point of view, the entire process is governed by two dominant phenomena: (1) intensive liquid evaporation near the heated surface in the superheated layer, leading to bubble growth, (2) natural convection resulting from bubble movement [2].

Although the macroscopic aspects of this phenomenon are well documented, the essential details on the atomic and molecular scale remain largely

unknown [3]. Every change in geometric dimensions requires experimental investigation to identify correlations between the collected results under given measurement conditions. Depending on factors such as the type of boiling liquid, roughness and porosity of the material, and the width and depth of the minichannels, the heat transfer coefficient may vary in unpredictable ways. For example, increasing the height or width of the minichannels does not necessarily lead to improved heat transfer performance.

2 Experimental Setup

The experiment was carried out using a modified measurement setup (Fig. 1a), developed on the basis of designs described in [4–6]. The main module of the experimental setup (Fig. 1b) enabled temperature recording using eight type K thermocouples. Two of them (T1 and T2) measured the temperature of the working liquid that fills the cylindrical glass vessel. The condenser ensured that the atmospheric pressure was maintained during the measurements and allowed the condensate to return to the vessel. Four thermocouples (T5–T8), placed inside the copper heating cylinder (7b), allowed one to determine the heat flux generated by the cartridge heater (8b). Two additional sensors (T3 and T4), located in grooves below the sample, were used to determine superheating. Sample (5b) was soldered with a layer of tin to the copper heating cylinder. An autotransformer (3a) equipped with a wattmeter (2a) enabled adjustment and preliminary determination of the power supplied to the sample. A constant saturation

* Corresponding author: ndadas@tu.kielce.pl

temperature of the liquid during the experiment indicated that the system pressure remained stable.

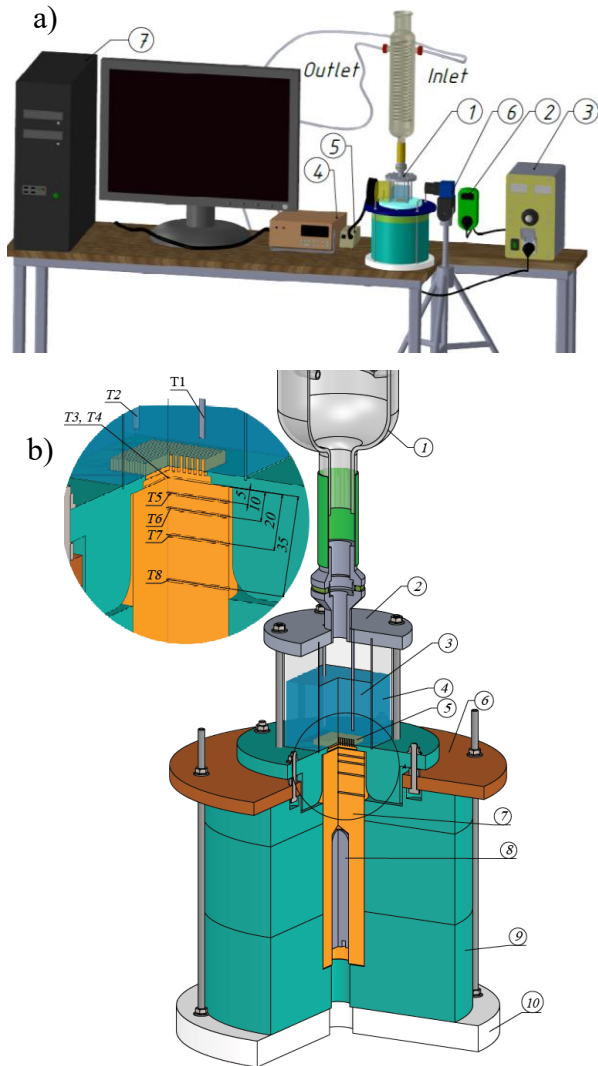


Fig. 1. a) Measurement setup: 1 – main module, 2 – wattmeter, 3 – autotransformer, 4 – data acquisition station, 5 – KL 2500 LED fiber-optic illuminator, 6 – high-speed camera, 7 – computer; b) main module: 1 – condenser, 2 – aluminum housing, 3 – working fluid, 4 – glass vessel, 5 – sample, 6 – reinforcing flange, 7 – copper cylinder, 8 – cartridge heater, 9, 10 – insulation.

The sample MC (with minichannels 5.5 mm deep, 1 mm wide), which was soldered to the heating cylinder, was modified by placing either copper foam or copper mesh inside its channels. Figure 2 presents the characteristic dimensions used to identify the samples listed in Table 1. The filling material was placed in the minichannel space by pressing. The forces resulting from bubble interactions with the surface during pool boiling were sufficiently small to prevent any displacement of the inserted elements during the experiments. The fabricated microchannels increased the heat transfer surface area, thus improving the heat transfer coefficient and heat flux. The addition of porous elements enabled capillary wicking of the liquid and contributed to an increase in the number of nucleation sites and more efficient removal of vapor bubbles from the minichannels during boiling.

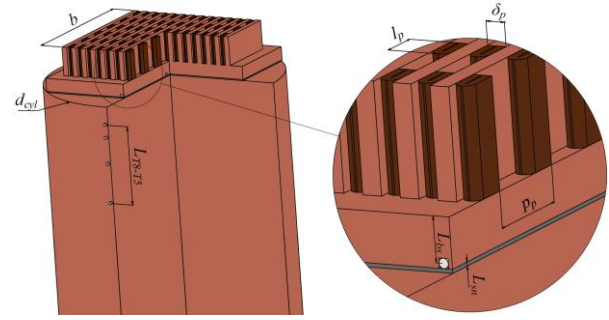


Fig. 2. Heating cylinder with an example of a soldered sample, where d_{cyl} – diameter of the heating cylinder [m], b – side length of the square sample [m], L_{bs} – distance from the thermocouple axis to the bottom of the minichannels [m], L_{sn} – distance between the heating cylinder and the sample, filled with tin [m], L_{T8-T5} – distance between thermocouples T5 and T8 [m].

Table 1. Sample designations and their characteristic dimensions.

Oznakowanie próbki	a , m	l_p , m	p_p , m	δ_p , m	n
MC	-	-	-	-	-
MCC-M-3-0.5-2	0.3	2	3	0.5	2
MCC-M-3.5-0.5-2	0.3	2,5	3.5	0.5	2
MCC-F-3.6-0.3-3	0.25	1,5	3.6	0.3	3
MCC-F-4.2-0.5-2	0.25	2	4.2	0.5	2

where: F – copper foam, M – mesh, a – mesh aperture/pore size [m], l_p – length of a single porous insert [m], p_p – pitch (distance between consecutive inserts) [m], δ_p – thickness of copper mesh/foam [m], n – number of porous elements placed side by side [-].

To determine the boiling curves (Fig. 3), the following relations were applied:

The heat flux was calculated using the following equation:

$$q = \lambda_{Cu} \frac{T8-T5}{L_{T8-T5}} \cdot \frac{\pi d_{cyl}^2}{4b^2} \quad (1)$$

where: λ_{Cu} – thermal conductivity of copper [$Wm^{-1}K^{-1}$], $T8$, $T5$ – temperatures measured by the respective thermocouples [K].

The heating surface temperature was determined from:

$$T_{pg} = \frac{T3+T4}{2} - q \left(\frac{L_{bs}}{\lambda_{Cu}} + \frac{L_{sn}}{\lambda_{Sn}} \right) \quad (2)$$

where: $T3$, $T4$ – temperatures measured by the respective thermocouples [K], λ_{Sn} – thermal conductivity of tin [$W m^{-1} K^{-1}$].

Superheat was defined as:

$$\Delta T = T_{pg} - \frac{T1+T2}{2} \quad (3)$$

where: $T1$, $T2$ – temperatures measured by the respective thermocouples [K].

The heat transfer coefficient was then determined from

$$\alpha = \frac{q}{\Delta T} \quad (4)$$

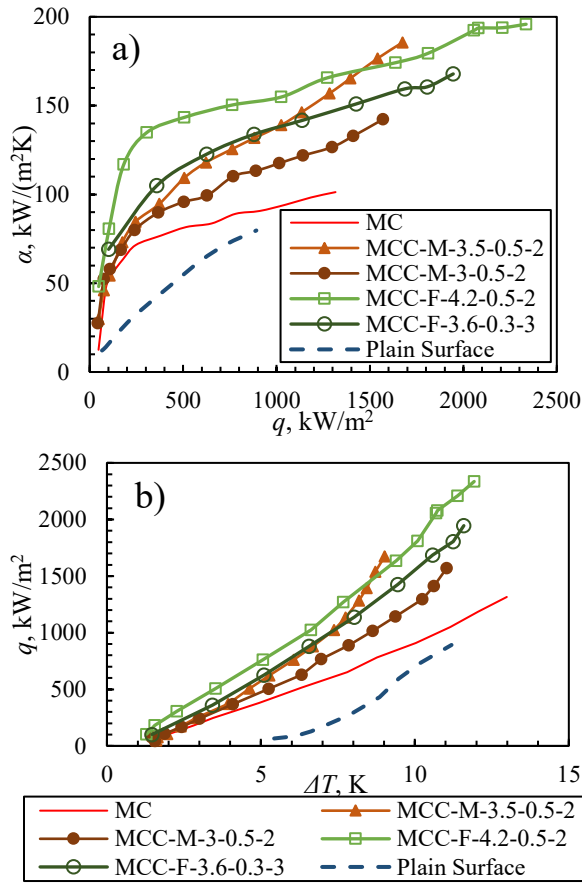


Fig. 3. Boiling curves: a) heat transfer coefficient as a function of heat flux density, b) heat flux density as a function of superheat.

Analyzing the curves presented in Fig. 3, it can be observed that for surfaces with minichannels filled with foam or copper mesh, a significant increase in the heat transfer coefficient and heat flux was obtained compared to the smooth surface and the surface with empty minichannels (MC). For the smooth surface, the maximum heat transfer coefficient was approximately $80 \text{ kW}/(\text{m}^2\text{K})$, while for the MC-F-4.2-0.5-2 sample, it reached about $200 \text{ kW}/(\text{m}^2\text{K})$ (a 2.5-fold increase). The maximum heat flux density for the smooth surface was around $900 \text{ kW}/\text{m}^2$, while for the MC-F-4.2-0.5-2 surface, it reached approximately $2300 \text{ kW}/\text{m}^2$ (also about a 2.5-fold increase).

3 Determination of the detaching bubble diameter

The diameter of the bubble is related to the properties of the fluid, the superheat of the surface, and the geometry of the surface. With the size and frequency of the detaching bubbles as well as the density of nucleation sites, it is possible to analytically determine the heat flux density. To verify the calculation assumptions with the experiment, a visualization of the boiling process was performed, and the diameter of the detaching vapor bubbles was determined (Fig. 4). The process was recorded using a high-speed camera (210 frames per second).

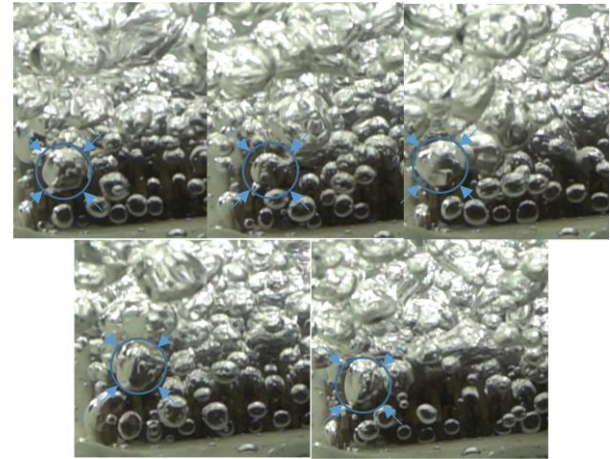


Fig. 4. Example of boiling visualization with bubble size determination for the MCC-F-4.2-0.5-2 surface (with water as the working fluid) at a superheat of 1.3 K.

To determine the diameter of the detaching bubble, a balance of six forces was applied (Fig. 5):

- Buoyancy force (F_{bu}),
- Inertia of the vapor bubble (F_{bi}),
- Surface tension force (F_{st}),
- Drag force (F_d),
- Pressure difference force (F_{pr}),
- Liquid inertia force (F_{li}).

The detailed dimensions and directions of the acting forces are shown in Fig. 5.

The forces mentioned above were calculated using the following relationships:

Buoyancy force:

$$F_{bu} = \frac{\pi d_b^3}{6} (\rho_l - \rho_v) g \quad (5)$$

where: ρ_l – liquid density [kg m^{-3}], ρ_v – vapor density [kg m^{-3}], g – gravitational acceleration [m s^{-2}].

Bubble inertia force:

$$F_{bi} = \frac{\pi \rho_v d_b^4}{4 t_g^2} \quad (6)$$

where: the bubble growth time was determined by modifying the correlation proposed by Chien and Webb [7]:

$$t_g = 0,5 C_{tg}^{-1} \cdot \left[\frac{7 \rho_l T_{sat}}{\pi \rho_v i_{lv} \Delta T} \cdot (d_b^2 - w^2) \right]^{0,5} \quad (7)$$

where: T_{sat} – saturation temperature [K] and the coefficient $C_{tg} = 0.0296$.

Surface tension force:

$$F_{st} = \sigma L_c \cdot \sin(\theta) \quad (8)$$

where: σ – surface tension [N m^{-1}], and the length of the contact line L_c was determined similarly to [4]:

$$L_c = 4 \sqrt{\frac{7}{3} d_b^2 - \frac{8}{3} d_c w + \frac{1}{3} w^2} \quad (9)$$

Drag force:

$$F_d = 0,5 C_d \rho_l \left(\frac{dR}{dt} \right)^2 0,25 \pi d_b^2 \quad (10)$$

where: dR/dt is the bubble growth rate. The drag coefficient C_d was determined on the basis of the Reynolds number associated with the bubble growth velocity [8]:

$$C_d = \frac{5360}{Re^{0,79}} \quad (11)$$

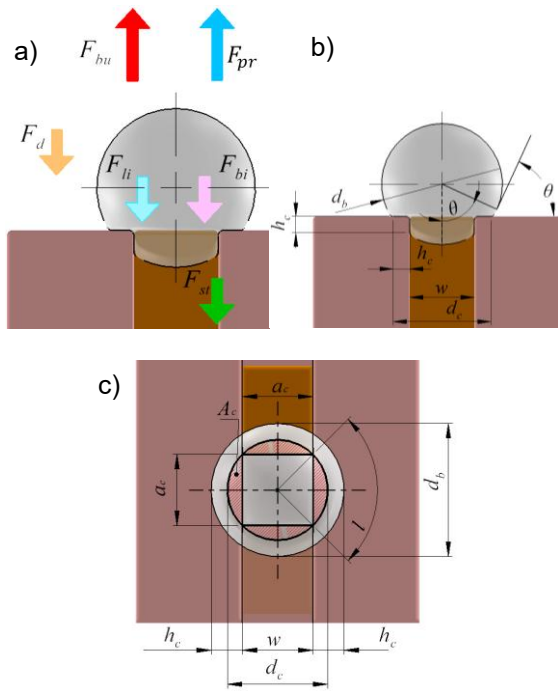


Fig. 5. a) Graphical representation of the forces acting on a vapor bubble; notation of geometric parameters: b) view along the minichannel, c) view perpendicular to the minichannel; where: d_c – contact diameter of the vapor bubble [m], h_c – contact height of the vapor bubble [m], d_b – vapor bubble diameter [m], a_c – chord length of the bubble diameter [m], l – arc length of a single contact surface [m], w – width of the minichannel [m], θ – contact (wetting) angle [rad], A_c – single contact area of the vapor bubble with a fin or porous filling [m²].

The pressure difference force was calculated according to the relationships presented in [4, 8–9]:

$$F_{pr} = \left(\frac{4\sigma}{d_b} + \rho_l \cdot \frac{d_b}{6} \frac{d^2 R}{dt^2} + \frac{c_d \rho_l}{8} \left(\frac{dR}{dt} \right)^2 \right) A_c \quad (12)$$

The contact area was determined from geometric relationships:

$$A_c = 2 \cdot (l - a_c) d_b + 2 a_c h_c \quad (13)$$

Liquid inertia force:

$$F_{li} = \frac{\pi d_b^3}{6} \rho_l \frac{d^2 R}{dt^2} \quad (14)$$

where $d^2 R/dt^2$ is the acceleration associated with bubble growth.

From the force balance $F_p + F_{bu} = F_{st} + F_{bi} + F_{li} + F_d$ and using the relationships given above, the diameters of the detaching bubbles were calculated numerically as a function of superheat. The results were compared with the diameters determined experimentally. The smallest and largest measured diameters (marked in red), as well as the averaged values (green curves), were selected for analysis. The diameters computed from the force balance were comparable to the mean values of the measurements. A comparison for four minichannel surfaces partially filled with mesh or copper foam segments is shown in Fig. 6.

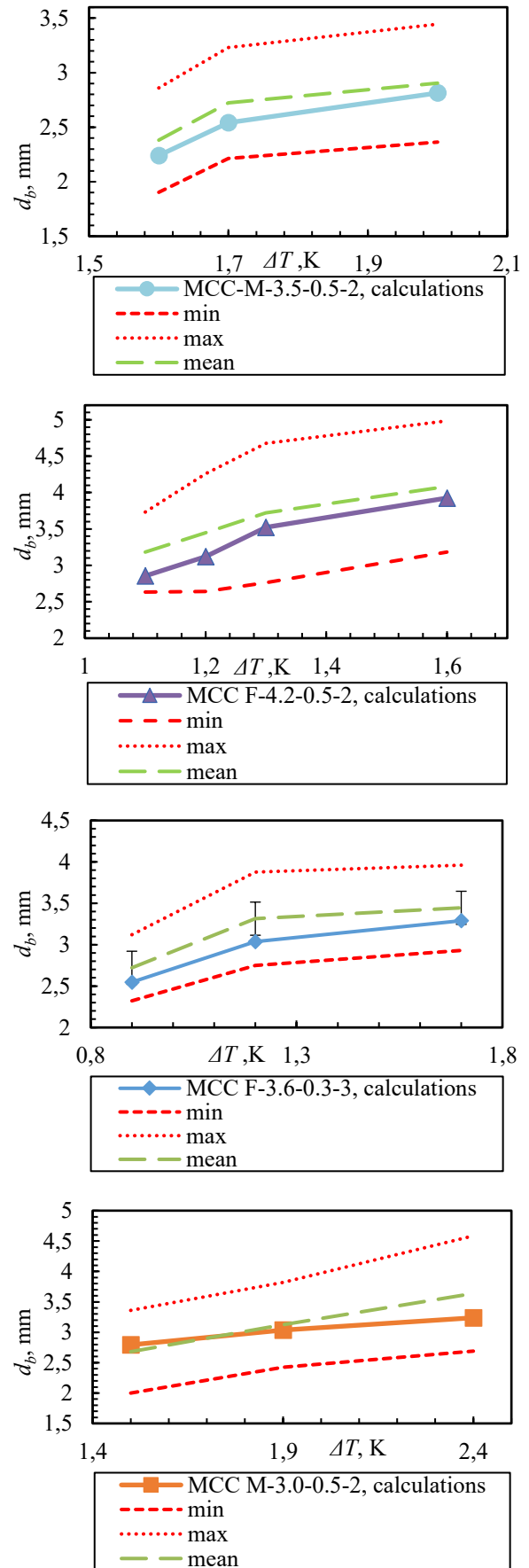


Fig. 6. Comparison of the detaching bubble diameters determined from visualization and calculations for selected samples.

The largest discrepancy between the mean bubble diameters obtained from the experiment and from the calculations was about 10 %, while the smallest was about 3 %. In all analyzed cases, clear differences are visible between the minimum and maximum bubble diameters, which increase with growing superheat and with larger diameters. The highest absolute discrepancy (1.9 mm) was recorded for the MCC-F-4.2-0.5-2 sample.

4 Conclusions

The study demonstrated that surfaces with minichannels partially filled with porous structures allowed for a two-fold increase in the heat transfer coefficient at a heat flux density of approximately 900 kW/m² and a three-fold increase at 500 kW/m², compared to the smooth surface. The diameters of the detaching bubbles, determined from visualization of the boiling process, increased with increasing superheat, which was consistent with the analytical model based on the balance of six forces acting on the vapor bubble. The diameters calculated from the model showed a maximum deviation of up to 11 % relative to the average values obtained from the experiment.

References

1. A. Salehi, S. Mortazavi, M. Amin, A numerical study of heat transfer in saturated nucleate pool boiling process: a new analysis based on the inherent physics. *Acta Mech.*, **233(9)**, 3601–3622 (2022). <https://doi.org/10.1007/s00707-022-03290-8>
2. J. Kim, Review of nucleate pool boiling bubble heat transfer mechanisms. *Int. J. Multiph. Flow*, **35(12)**, 1067–1076 (2009). <https://doi.org/10.1016/j.ijmultiphaseflow.2009.07.008>
3. X.-W. Lin, W.-T. Wu, Y.-B. Li, D.-W. Jing, B. Chen, Z.-F. Zhou, Recent advances of molecular dynamics simulation on bubble nucleation and boiling heat transfer: A state-of-the-art review. *Adv. Colloid Interface Sci.*, **334**, 103312 (2024). <https://doi.org/10.1016/j.cis.2024.103312>
4. R. Pastuszko, R. Kaniowski, N. Dadas, M. Bedla-Pawlusek, Pool boiling enhancement and a method of bubble diameter determination on surfaces with deep minichannels. *Int. J. Heat Mass Transf.*, **179**, 121713 (2021). <https://doi.org/10.1016/j.ijheatmasstransfer.2021.121713>
5. N. Dadas, R. Pastuszko, R. Kaniowski, Pool boiling heat transfer on minichannels with porous structure. *EPJ Web of Conf.*, **264**, 01010 (2022). <https://doi.org/10.1051/epjconf/202226401010>
6. R. Pastuszko, N. Dadas, R. Kaniowski, Pool boiling of Novec-649 on minichannels filled with copper foam. *EPJ Web of Conf.*, **264**, 01028 (2022). <https://doi.org/10.1051/epjconf/202226401028>
7. L.-H.Chien, R. L. Webb A nucleate boiling model for structured enhanced surfaces. *Int. J. Heat Mass Transf.*, **41(14)**, 2183–2195 (1998). [https://doi.org/10.1016/S0017-9310\(97\)00302-5](https://doi.org/10.1016/S0017-9310(97)00302-5)
8. H. Beer, Das dynamische Blasenwachstum beim Sieden von Flüssigkeiten an Heizflächen. *Forsch. Ingenieurwes.*, **37(3)**, 85–90 (1971). <https://doi.org/10.1007/BF02558738>
9. W. Ding, J. Zhang, D. Sarker, U. Hampel, The role of microlayer for bubble sliding in nucleate boiling: A new viewpoint for heat transfer enhancement via surface engineering. *Int. J. Heat Mass Transf.*, **149**, 119239 (2020). <https://doi.org/10.1016/j.ijheatmasstransfer.2019.119239>